Development of Aluminium-Titanium Tube Joints for Space Propulsion Systems

Andrew Norman, Arnau Bernad** and Stefan Resch****
**European Space Agency*
Keplerlaan 1, PO Box 299, 2201AZ Noordwijk, The Netherlands
*** Omnidea-RTG*
Handelshof 26, 28816 Stuhr, Germany
**** IWS-Service*
Berliner Tor 13, 20099 Hamburg, Germany

Abstract
The welding technique of Rotary Friction Welding (RFW) has been used to successfully develop an aluminium-titanium ¼" tube-to-tube joint. By varying the profile across the weld geometry, and developing an understanding of the main processing conditions, it was possible to optimise the welding process such that high integrity welds were consistently produced. For the optimised welds, failure of the weld always occurred on the aluminium side of the weld, in the heat affected zone (HAZ). Failure at the weld interface was never observed. The tensile strength of the welds was comfortably above the required minimum of 260 MPa, and each of the welded joints survived thermal cycling, vibration and burst pressure testing.

1. Introduction

Propellant and pressurant tanks are used across all satellites and spacecraft as part of the propulsion system, and require high levels of mechanical properties coupled with low mass. Propellant tanks are commonly used to store liquids such as Hydrazine, and generally do not have to withstand pressures greater than 25 bar. Due to their size, propellant tanks are typically made from Titanium forgings and are manufactured using a combination of electron beam and TIG welding. However, the ESA Directive "Design for Demise" has been introduced in 2008, which states: "What goes up must completely burn up – or 'ablate' – during uncontrolled atmospheric re-entry as a means of post-mission disposal" [1]. Although Ti-6Al-4V is an excellent material for the manufacturing of propellant tanks, titanium has a melting point of around 1600°C which is the same order of magnitude as the maximum temperature reached by the spacecraft during re-entry. Therefore there is the danger that during uncontrolled re-entry, parts of the spacecraft including the propellant tanks may survive. There is therefore a need to find an alternative material to Titanium for the manufacturing propellant tanks which will burn up during re-entry. One such material is aluminium, some alloys of which have already been used for the external oxygen tank of the Space Shuttle. If Aluminium propellant tanks are successfully introduced in space propulsion systems, it will be necessary to interface such tanks with the tubing and pipework surrounding the tank. As such pipework will still be made from titanium alloys, usually Ti-6Al-4V or Ti3Al2.5V, it is necessary to consider how to join an aluminium tank with titanium tubing.

In contrast to propellant tanks, pressurant tanks, such as those used to store Xenon, are also manufactured using titanium, although due to the higher operating pressure, the titanium is used as a liner and the tank is overwrapped with a composite (COPV). As the loading is taken by the composite overwrap, the liner material only needs to be leak tight, and could therefore be manufactured from alternative materials. Omnidea Limitada is developing a new process which will enable the titanium liner to be replaced with aluminium using a single step forming operation [2]. If this type of tank is successfully introduced, it will also be necessary to consider how to join an aluminium tank with titanium tubing. Therefore in order to successfully develop an aluminium-titanium tube-to-tube joint, an ESA GSTP funded activity was started in 2011 together with Omnidea (Portugal), Omnidea-RTG (Germany) and IWS (Germany).

2. Welding Technique Selection and Parameter Development

A review of the prior work performed on developing transition joints between materials with very different melting points such as aluminium and titanium, quickly showed that it is very difficult, if not impossible, to produce high quality welds using conventional fusion welding techniques. The composition of any fusion weld is highly asymmetrical and contains a number of intermetallic compounds (Ti_3Al, TiAl and $TiAl_3$) which are brittle in nature and compromise the strength of the weld [3]. Consequently, attention was focused on welding techniques which were performed in the solid state. Using Friction Stir Welding, Chen *et al* [4] demonstrated that it was possible to produce a lap joint between the aluminium alloy LF6 and titanium alloy TC1, although such a geometry could not be easily adapted for a tube-to-tube joint. Other techniques such as Cold Pressure welding, Ultrasonic Welding and Explosive Welding have also been tried for different material combinations, and though joints can be successfully produced, these techniques are not very suitable for producing a tube-to-tube joint.

The conclusion of the literature review was that for tube-to-tube type applications, the most suitable welding technique was that of Rotary Friction Welding. In a previously ESA funded activity, this technique had already been successfully applied to the development of stainless steel-aluminium tube-to-tube joints of a similar size [5].

2.1 Rotary Friction Welding

Rotary Friction Welding is an ideal solid-state welding process which can be used to weld together cylindrical material rods, in which the heat is produced by the relative motion of the two interfaces being joined. This method relies on the direct conversion of mechanical energy into thermal energy via surface friction to form the weld, without any other existing source of heat. As a solid-state welding process, it involves no melting of the involved materials.

Figure 1 shows a typical rotational friction weld in which one material rod is held fixed while the counterpart to be welded on is being rotated. The work pieces are brought together under an axial force. The principal parameters include the rotation speed, the pressure force, and the welding time. These parameters govern the heat generation and thus the weld. Finally, the rotation is rapidly or gradually stopped, and the axial force increased in the forging phase, when atomic diffusion occurs in the interfaces in contact, allowing a metallurgical bond to form between the two materials.

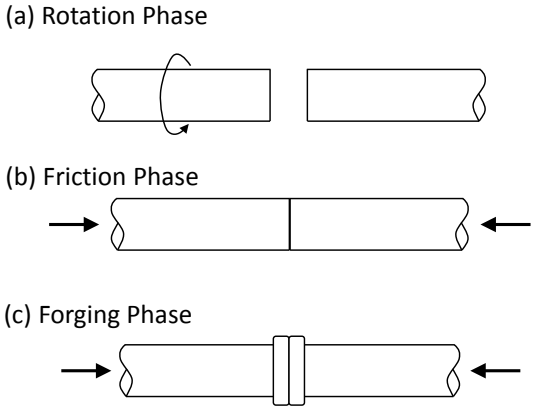

Figure 1: Schematic diagram showing the three stages of the Rotary Friction Welding process.

Due to the complex nature of the welding process which involves heat generation through friction and abrasion, heat dissipation, plastic deformation and chemical inter-diffusion, it is very difficult to accurately develop predictive models or simulation tools. From a qualitative perspective, the RFW process is well understood through empirical studies. The main parameters which need to be controlled during the process are:

- Relative velocity (rotational speed)
- Applied pressure (welding force and pressure force)
- Welding time and pressing time
- Surface temperature (consequence of pressure and time)
- Bulk material properties
- Surface condition and presence of surface films, coatings or oxide layers.

The rotational speed, the applied pressure, and the duration of the force are the three variables that are controlled during the welding process. The surface temperature is the critical parameter for ensuring good welds, and is dependent on the processing conditions and the materials being joined.

There are two principal methods which can be used for RFW: Direct-drive RFW (also known as conventional friction welding), and Inertia-drive RFW (also known as flywheel friction welding). Direct-drive RFW uses a motor running at constant speed to provide energy to the weld, whereas Inertia-drive RFW stores the energy in an inertia flywheel which is later transferred into the weld. In principle, both approaches are capable of providing similar quality results if the correct procedure can be developed. In this paper the Direct-drive RFW method is used as it is more suited to smaller applications and softer materials such as aluminium. The operation of a direct-drive machine consists of a friction phase where heat is generated, a stopping phase where the rotation is terminated, and a forging phase where the pressure is applied. It should be considered that the time required to stop the rotating part is also an important variable because it affects the weld temperature and the timing of the forging force. Figure 2 shows the relationship among the control variables for a typical Direct-drive RFW.

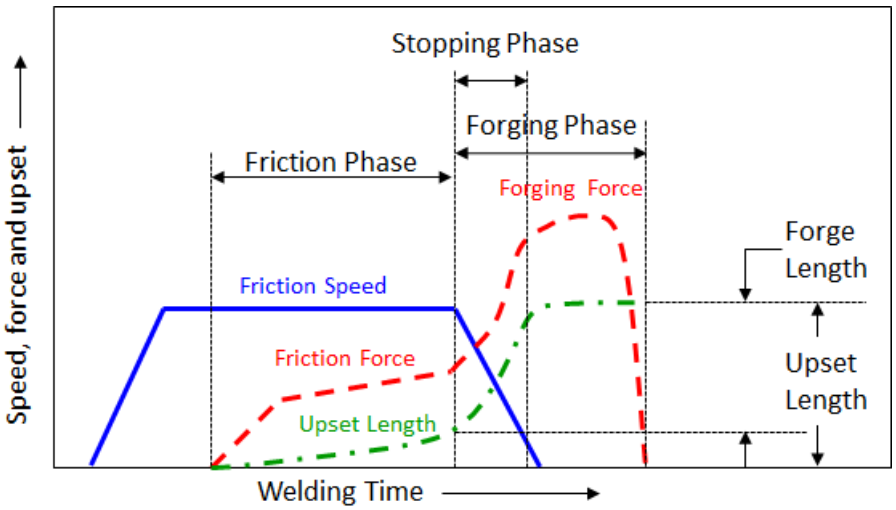

Figure 2: Generic plot of friction speed, axial force, and upset length vs time, relative to the three phases of the Direct-drive RFW process [6].

2.2 Materials Selection and Joint Dimensions

A trade-off was performed to evaluate different candidates for the aluminium and titanium alloys, taking into consideration how their characteristics would potentially facilitate the cold-welding process, as well as the suitability of these materials to meet the requirements of the intended application. The materials selected for the tube-to-tube joints were AA6082-T651 12mm diameter rods and Ti-6Al-4V 8mm diameter rods. After welding, the outer diameter of each tube-to-tube joint was machined to 6.35mm (¾") with a wall thickness of 1.5mm (inner diameter = 3.35 mm). The final length of each tube-to-tube joint was 70 mm.

2.3 Welding Parameter Development

In order to identify the optimum welding parameters, and the window in which high quality defect free welds could be produced, a number of welding trials were performed. The welding parameters were varied within the window shown in Table 1, overleaf. Prior to welding, the ends of the rods were shaped in order to improve the joint integrity. Some examples of the first welding trials are shown in Figure 3, overleaf. The performance of each weld was assessed by measuring the tensile strength. In addition some metallographic examination was performed to establish the alignment after welding, and the nature of the weld interface. One key observation from the initial welding trials was a misalignment in the welded joint. As this occurred in all samples, it was concluded that although the chosen welding parameters had a certain influence on the amount of misalignment, the root cause had to be structural. Analysis of the machine revealed that during welding, the region below the welding area was bending slightly under the high forces of the friction and forging phases of the welding process. The machine was therefore stiffened by

adding a structural frame which allowed the counter forces to be equally distributed in the machine, thus maintaining the alignment of the welded coupons, even under the large forging force.

Table 1: Process parameters used in the initial welding Trials

Parameter	From	To
Rotational Speed	6,000 rpm	14,000 rpm
Contact Force	500 N	500 N
Friction Force	9.0 kN	18.0 kN
Friction Time		3,000 ms (maximum)
Forging Force	13.0 kN	30.0 kN
Forging Time	250 ms	2500 ms

Figure 3: Exampless of welded coupons prepared for tensile testing.

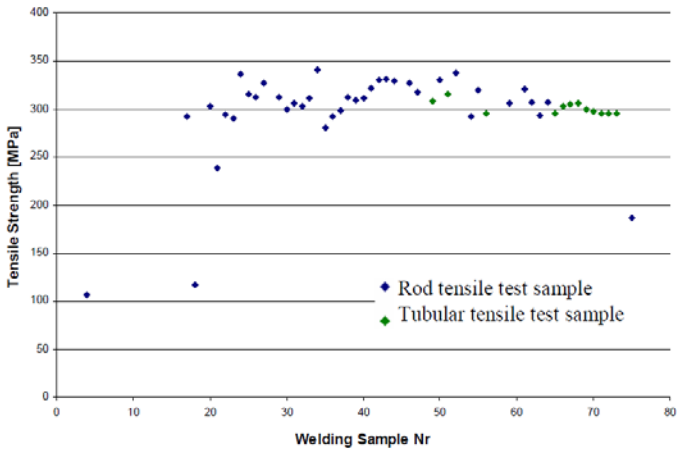

Figure 4: Summary of the tensile strength observed during the welding development phase.

In the initial welding trials, considerably variability was observed in the tensile properties as different configurations were tried. However once the conditions were more optimised, the measured tensile strength was around 310 MPa +/- 10 MPa (See Figure 4).

For the optimum welding parameters, the weld interface was very clean with no obvious brittle phases present (Figure 5a). Hardness profiles taken along both the aluminium and titanium sides of the welded joint (Figure 6) revealed that for the titanium side, the hardness was unaffected, whereas for the aluminium side, the lowest hardness

was at the interface (~ 80 Hv) which increased to around 110 Hv approximately 1mm from the interface. After mechanical testing, the welds always fractured on the aluminium size, in the HAZ (see Figure 5b).

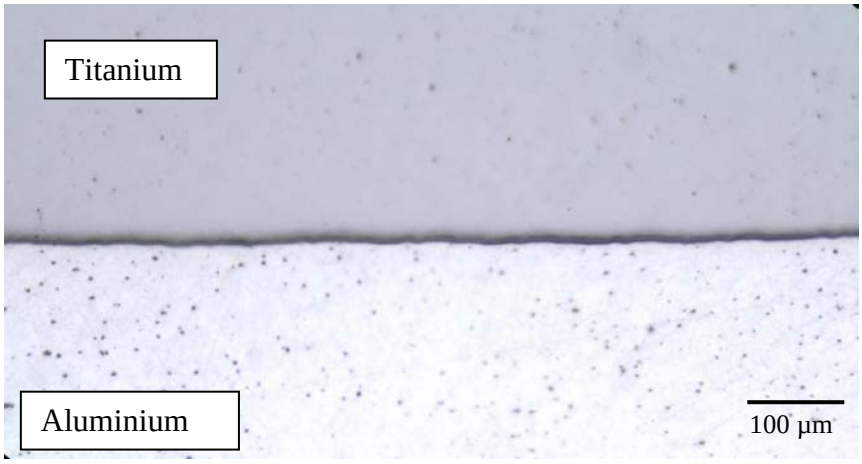

Figure 5: Example of the interface between the titanium and aluminium tube-to-tube joint.

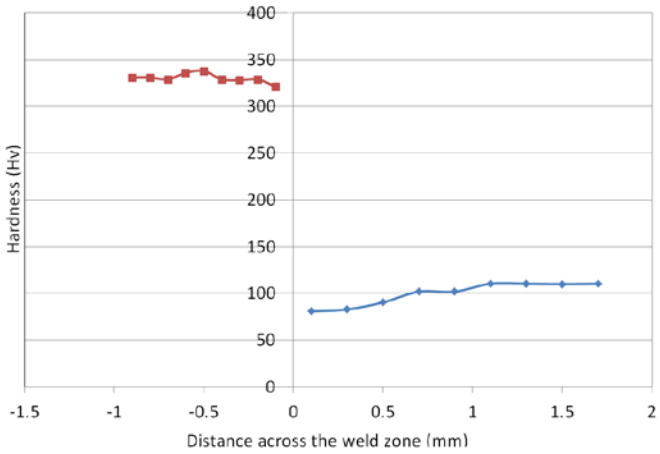

Figure 6: Hardness profile across one of the welded joints. (red) Titanium, (blue) aluminium.

In order to further understand the behaviour of the joint, additional tensile testing was performed together with the application of the ARAMIS Optical 3D Deformation Analysis [7]. This is a well established non-contact technique which allows the surface strain values (major and minor strain) and strain rates to be displayed visually on the sample surface. Figure 7 (overleaf) shows a series of time lapse images taken during the final stages of the tensile test, together with the magnitude of the strain in the test direction. Although the overall measured elongation of the tensile specimen was about 1.5mm, the amount of strain prior to breaking was, in some positions, close to 20%. The images in Figure 7 also demonstrate that although the strain is highly localised, a considerable amount of necking occurs and that failure occurs on the aluminium side of the joint, and not directly at the interface. This is in agreement with the hardness plot shown in Figure 6, where the weakest region was identified as being in the HAZ of the AA6082 part of the joint.

At the end of the weld development phase, it was possible to identify a set of optimum conditions, together with a reasonable processing window. The analysis of the metallography of the development samples showed generally no defects and so the process development was optimised using the mechanical performance of the joint.

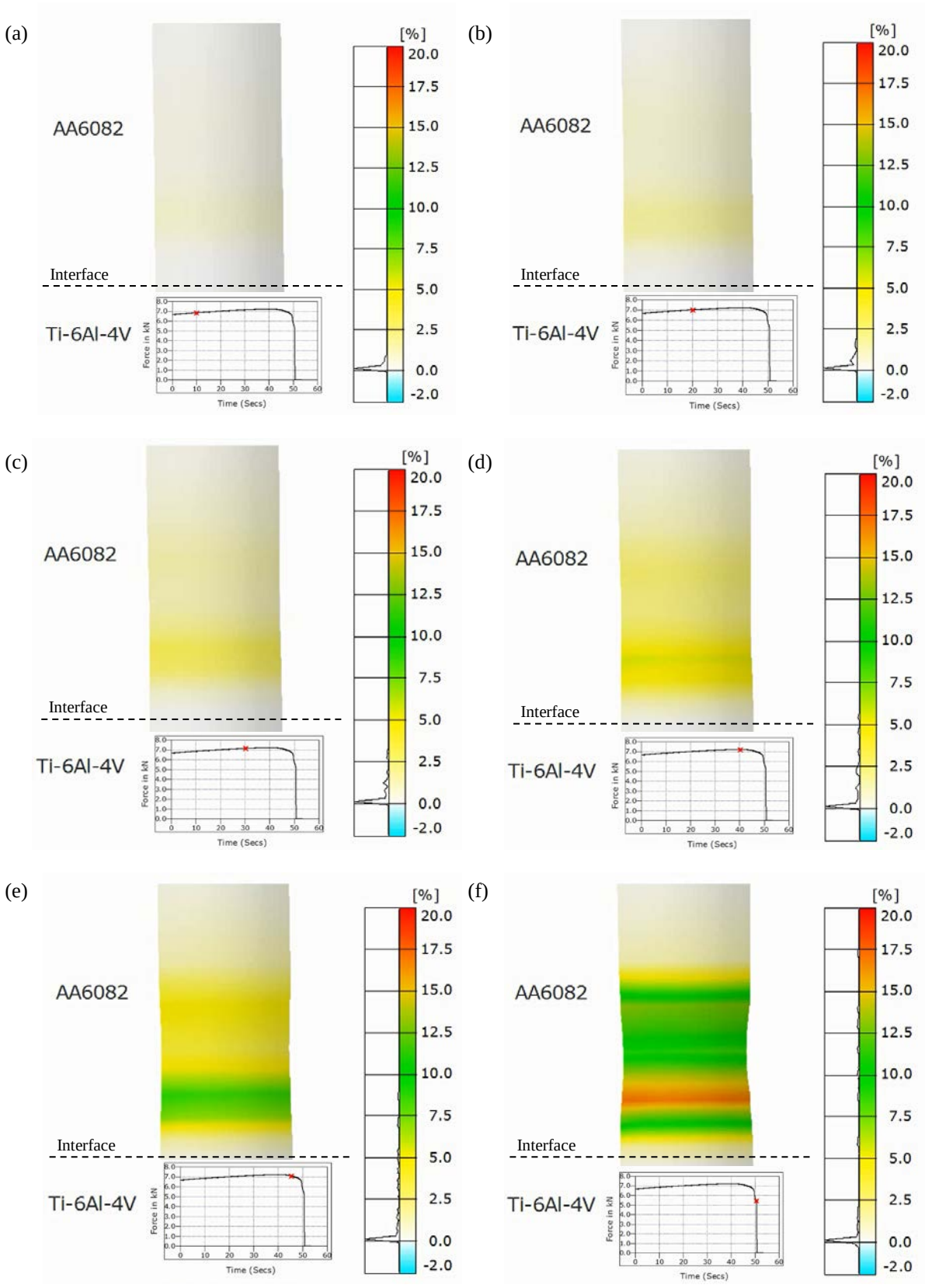

Figure 7: A sequence of time lapse images taken towards the end of the tensile test, showing the accumulation of strain in the testing direction.

3. Characterisation and Performance of Optimised Welds

Once a reliable set of welding parameters had been established, a total of 12 tube-to-tube welds were produced using the same conditions. Each tube-to-tube joint was subjected to a rigorous testing campaign consisting of visual inspection, pressure testing, dye penetrant inspection, leakage testing, thermal cycling and vibration testing. Three of the welded joints were then subjected to mechanical testing, three welded joints were subjected to burst, and three were subjected to microsectioning and metallographic inspection. The testing campaign is detailed in Figure 8.

3.1 Visual Inspection (Welds 1 to 12)

Each welded joint was visually examined for conformance with respect to workmanship, identification, markings and envelope dimensions. Special care was paid to identifying any material discolouration resulting from the electro-erosion process. The requirements to be met was that shall be no discolouration in the tube ends, that the outer diameter D = 6,35 mm ± 0,05 mm, and the inner diameter d = 3,35 mm ± 0,05 mm. For all of the welded joints, the dimensions met the requirements and no discoloration was observed. The results of the dimensional measurements are shown in Table 2.

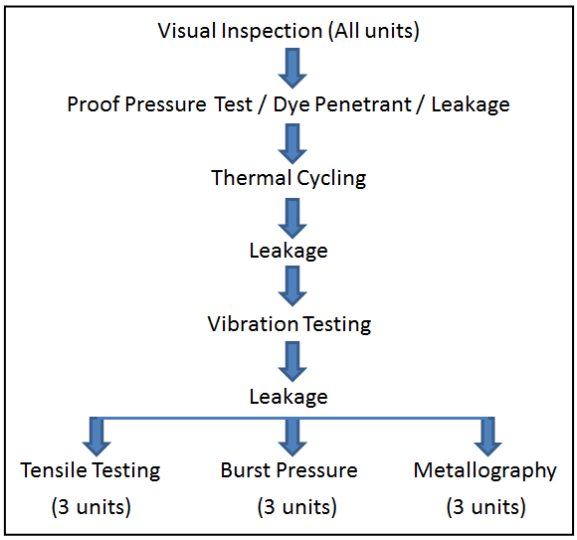

Figure 8: Flow chart showing the testing campaign

Table 2: Visual Inspection and Dimension Checks for the Welded Joints

Weld No.	Outer Diameter [mm]	Inner Diameter [mm]	Min. Wall Thickness [mm]	Max. Wall Thickness [mm]	Total Length [mm]
1	6,39	3,32	1,52	1,58	70,16
2	6,38	3,32	1,50	1,57	70,12
3	6,39	3,31	1,51	1,57	70,10
4	6,39	3,32	1,52	1,58	70,12
5	6,39	3,30	1,52	1,59	70,17
6	6,39	3,32	1,50	1,58	70,10
7	6,39	3,31	1,49	1,59	70,10
8	6,40	3,32	1,51	1,58	70,14
9	6,40	3,31	1,51	1,58	70,10
10	6,40	3,32	1,49	1,58	70,09
11	6,39	3,31	1,49	1,56	70,14
12	6,40	3,31	1,53	1,59	70,08

3.2 Proof Pressure Testing, Dye Penetrant and Leakage Testing (Welds 1 to 12)

Proof pressure testing, together with dye penetrant and leakage testing was performed immediately after visual inspection so that any obvious manufacturing defects were identified.

3.2.1 Proof Pressure Test

In this test, the proof pressure level was selected to be 1.5 times the MEOP which is in accordance with ECSS-E-ST-32-02C [8], Since the MEOP for the intended application was 300 bar, all welded joints were subjected to a proof pressure level of 450 bar and maintained for 5 minutes using hydraulic red oil [9]. For all the welded joints, no dimensional changes were observed after the proof pressure test.

3.2.2 Dye Penetrant Test

All the welded joints were submitted to a dye penetrant inspection in search for surface cracks both in the parent metal and in the weld area, which may have been widened by the previous proof pressure test. For all of the welded joints, no cracks were observed.

3.2.2 Leakage Test

The leakage test was performed with a Helium leak detector connected to vacuum chamber. Helium is applied at 170 bar to all test specimens, and the test is performed to 3 transition joints simultaneously, where the measured leakage would be the sum of all the present leaks. The requirement to be met is that the leak rate shall be $\leq 1\times10^{-6}$ scc/s. Should the requirement be violated in a test with multiple specimens, the test is then repeated with each specimen independently. The leakage test results are shown in Table 3 and for each test, the measured leak rate met the requirement.

Table 3: Leakage Test Results after Proof Pressure Test

Weld No.	Leak Rate (scc/s)
1, 2, and 3	3.58×10^{-7}
4, 5, and 6	$1{,}88\times10^{-7}$
7, 8, and 9	$5{,}13\times10^{-7}$
10, 11, and 12	$4{,}74\times10^{-7}$

3.3 Thermal Cycling Followed by Long Term Leak Testing (Welds 1 to 12)

Thermal cycling was performed on all units. A total of 4 cycles was performed under ambient pressure and internally pressurised at 200 bar. The maximum temperature reached was +80°C and the minimum temperature was -30°C, with a dwell time of 1 hour. During the cold cycles, the thermal chamber was flushed with dry air to avoid frost forming on the surface of the components, and the sensors. The experimental setup is shown in Figure 9 and the profile achieved is shown in Figure 10.

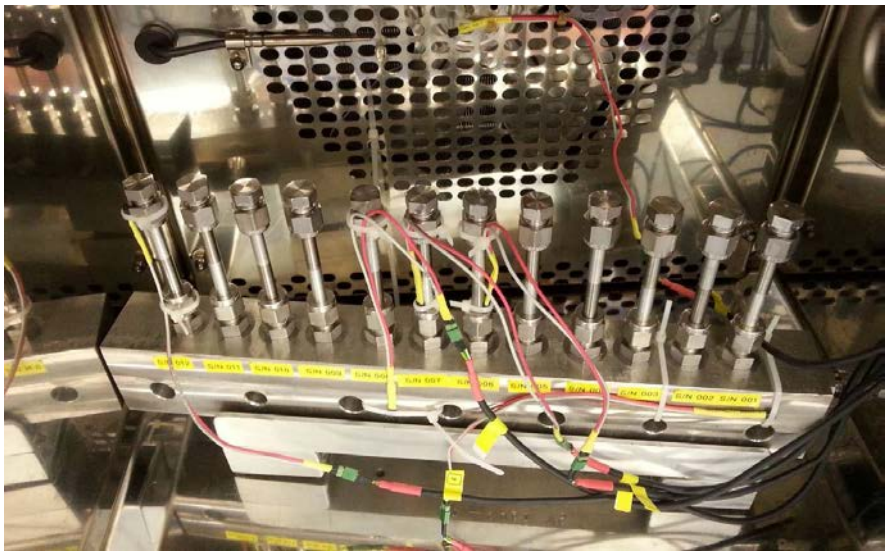

Figure 9: Experimental test set-up for the thermal cycling.

The leakage test performed after thermal cycling was performed using the long term leakage testing method. This consists of pressurizing the internal volume with a known gas, and measuring the pressure and temperature at the beginning and after a certain time, in this case after 91 hours. With this data, the total leakage rate of the internal volume can be calculated as follows:

From the initial and final conditions of pressure and temperature, the total amount of gas moles can be calculated with:

$$n_i = \frac{P_i.V}{R.T_i} \quad \text{and} \quad n_f = \frac{P_f.V}{R.T_f} \qquad [1]$$

From the difference between initial and final moles divided by test time, an average leakage rate in mol/s is obtained.

$$L\left[\frac{mol}{s}\right] = \frac{n_f - n_i}{t_{test}} \qquad [2]$$

The rate can then be converted to scc N_2/s if the amount of moles in an scc is known (4,46175 mol/scc), and then converted to scc He /s. For this experiment, P_i = 201.8 bar, P_f = 201.5 bar, T_i = 21.8°C and T_f = 21.4°C. This equates to a He leak rate of 1.76×10^{-6} which meets the requirement.

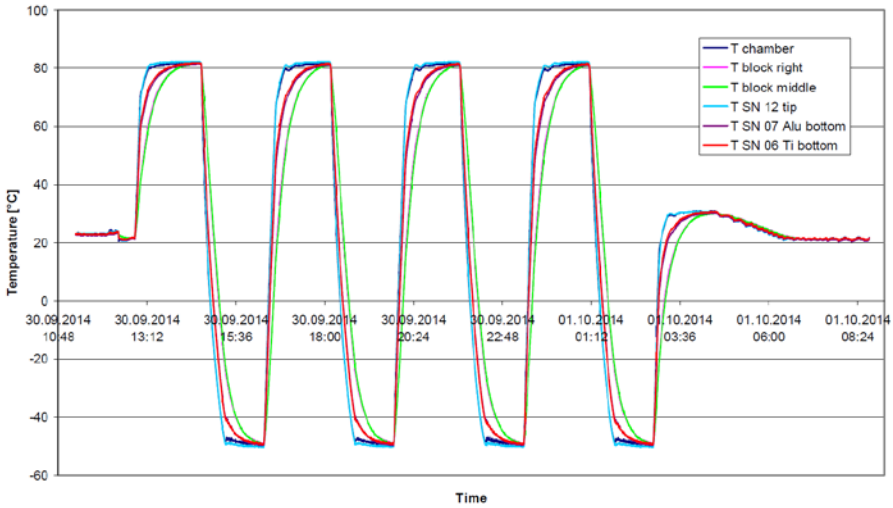

Figure 10: Plot showing the temperatures achieved during thermal cycling.

3.4 Vibration Testing Followed by Leak Testing (Welds 1 to 12)

The vibration test is performed to demonstrate that the joint shall withstand the defined mechanical loads without any damage or degradation. The sinusoidal vibration and random vibration qualification test levels and durations are specified in Table 6-2 of ECSS-E-ST-10-03C [10] and depend on the launcher specifications. In this test the unit is mounted to vibration test plate by a special fixture. All units were fixed on the titanium side and capped on their free end. The Swagelok connection and cap added 20g at the cantilever tip. In addition two welds (S/N 006, and 012) were equipped with an extra 100g mass at the cantilever tip (Figure 11).

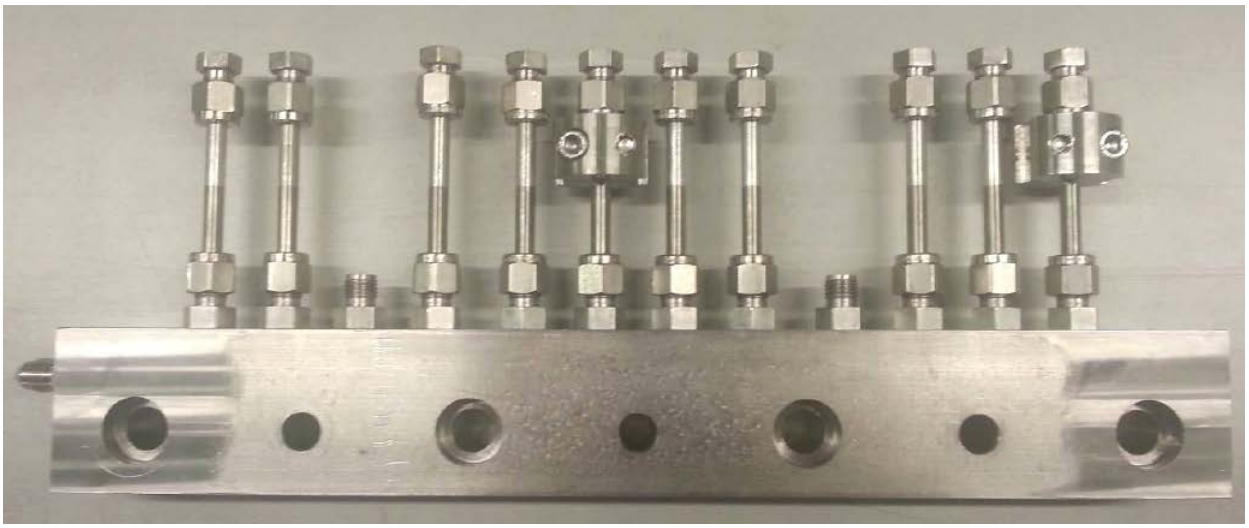

Figure 11: Experimental set-up for the vibration testing.

Sinusoidal resonance search was performed in each major orthogonal axis by slowly varying the applied frequency between 5 Hz and 2000 Hz with an input of 0,5 g and a sweep rate of 2 oct/min. Sinusoidal vibration was performed in each axis at a sweep rate of 4 oct/min with the following levels: 5-20 Hz – 11mm, 20-60 Hz – 20g, and 60-100 Hz – 6g. Finally, random vibration was performed according to the conditions given in Table 4 and Figure 12.

Table 4: Random Vibration Levels

Frequency Range [Hz]	Levels
20 - 100	+3 dB/oct
100 - 500	1.08 g^2/Hz
500 - 2000	-5 dB/oct
Test Duration	120 s
RMS in g	31.21

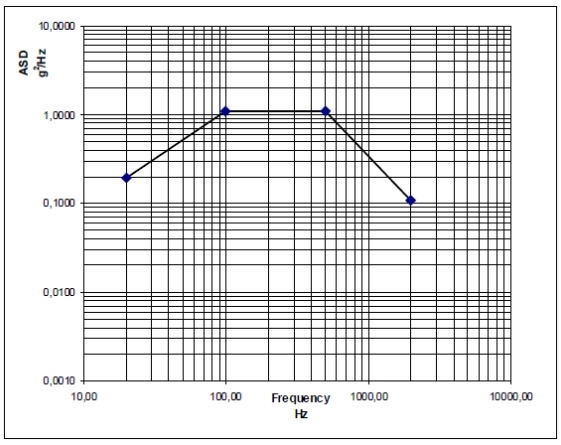

Figure 12: Random vibration spectrum.

3.5 Mechanical Testing (3 Welds)

Tensile testing was performed on three of the welded joints (01, 05 and 09) according to ISO 6892-1 [11], with the requirement that the minimum tensile strength is 260 MPa. The tensile strengths achieved were 327, 334, and 316 MPa respectively which comfortably meet the minimum requirement. This is approximately 90% of the tensile strength of the AA6082 alloy.

3.6 Burst Pressure Testing (3 welds)
According to ECSS-E-ST-32-02C [8], the welded joint can be classified as a Metallic Pressure Component (MPC), which then refers to the Table 4-5 of the mentioned standard indicating a Burst factor of 2.5. Three representative units of the batch (02, 10 and 12) were internally pressurized with increasing pressure until the maximum achievable pressure of the test set-up (around 1600 bar) was reached, without actually bursting the welded joint.

3.7 Microstructural Examinations (3 welds)
Three of the welded joints (03, 07 and 11) were subjected to microstructural examination. Each weld was sectioned in the vertical direction, mounted and polished using conventional techniques. Examples of the weld interface are shown in Figure 13.

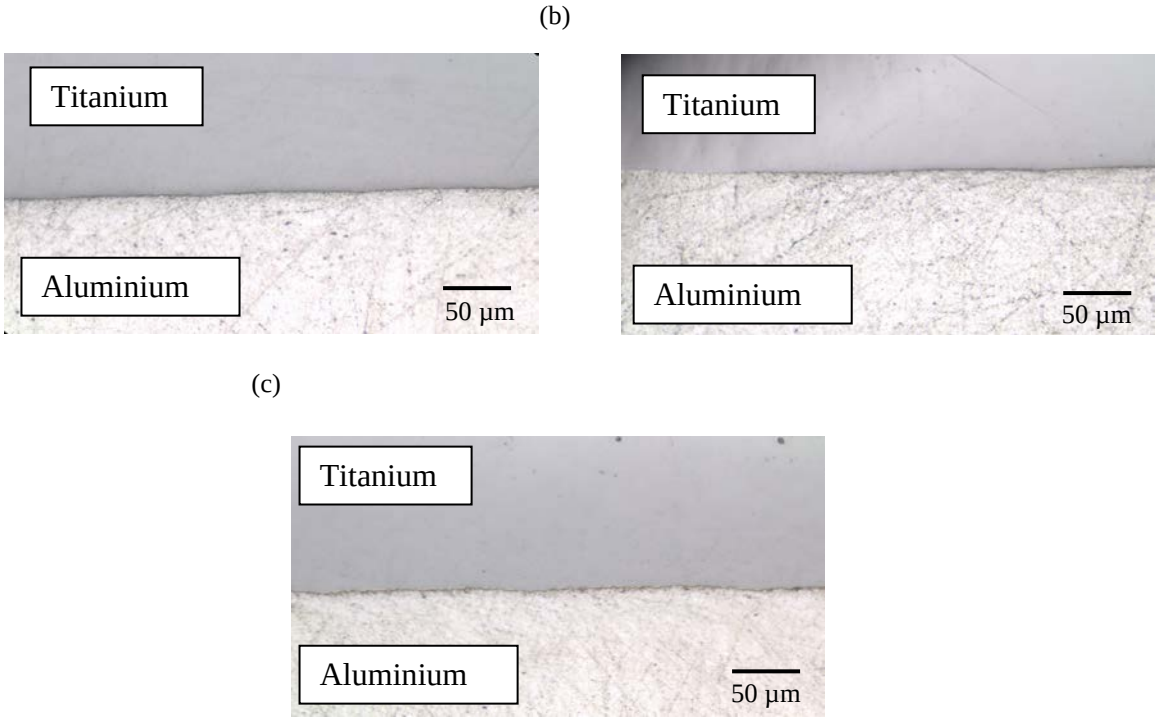

Figure 13: Interface of the aluminium-titanium welded joints for welds 03, 07 and 11.

4. Conclusions

The solid state welding technique of Rotary Friction Welding (RFW) has been used to successfully develop an aluminium-titanium ¼" tube-to-tube joint. The welding process was optimised by varying the main welding parameters including the rotational speed, applied pressure (welding force and pressure force) and welding time and pressing time. For the optimised welds, failure of the weld always occurred on the aluminium side of the weld, in the heat affected zone (HAZ). Levels of strain approaching 20% was seen in parts of the welded joint, with significant amounts of necking occurring on the aluminium side of the joint. Failure at the weld interface was never observed. The tensile strength of the welds was comfortably above the required minimum of 260 MPa, and in many cases reached around 320 MPa (approximately 90% of the weld strength of the aluminium alloy). Furthermore, in an extensive evaluation programme, each of the welded joints survived thermal cycling, vibration and burst pressure testing.

5. Acknowledgements

This work is performed under the ESA contract No. 4000111471/14/NL/PA, Alu-Ti Welding Demonstration and Pre-Qualification. The authors would also like to thank N. Fernandes and T. Pardal for helpful discussions.

6. References

[1] Space Debris Mitigation Guidelines of the Scientific and Technical Sub-Committee of the Committee on the Peaceful Uses of Outer Space, Annex IV of A/AC.105/890, UNCOPUOS, 06 March 2007.

[2] Alves, L.M., Santana, P., Fernandes, N., Moreira, H., Pardal, T., and Martins, A.F. 2015. Weldless liners for high pressure storage COPV. In Space Propulsion 2012, Bordeaux, France.

[3] Korenyuk, Y.M. 1975. Interaction of liquid aluminium and solid titanium in fusion welding, *Welding Production*. 22(6): 3−5.

[4] Chen, Y., Liu, C., and Liu, G. 2011. Study on the Joining of Titanium and Aluminium Dissimilar Alloys by Friction Stir Welding, *Open Materials Science Journal*. Vol.5.

[5] ESA contract No.21099-07-NL-EM, Titanium to Stainless Steel Transition Joints.

[6] Elmer, J.W. and Kautz, D.D. Fundamentals of Friction Welding. 1993. *ASM Handbook, Vol. 6, Welding, Brazing and Soldering, ASM International.*

[7] http://www.gom.com/metrology-systems/system-overview/aramis.html

[8] ESA, Space Engineering – Structural design and verification of pressurized hardware, ECSS-E-ST-32-02C Rev.1 (15/11/2008).

[9] Performance Specification Hydraulic Fluid, Petroleum base, Aircraft, Missile, and Ordnance, MIL-PRF-5606H (07/06/2002).

[10] ESA, Space Engineering – Testing, ECSS-E-ST-10-03C (01/06/2012).

[11] Metallic Materials – Tensile Testing – Part 1: Method of test at room temperature, ISO 6892-1 (15/08/2008).